Applied Catalysis B: Environmental 217 (2017) 201–213

Contents lists available at ScienceDirect

Applied Catalysis B: Environmental

journal homepage: www.elsevier.com/locate/apcatb

Review

Alloy *vs.* intermetallic compounds: Effect of the ordering on the electrocatalytic activity for oxygen reduction and the stability of low temperature fuel cell catalysts

Ermete Antolini

Scuola di Scienza dei Materiali, Via 25 aprile 22, 16016 Cogoleto, Genova, Italy

ARTICLE INFO

Article history:
Received 30 March 2017
Received in revised form 23 May 2017
Accepted 27 May 2017
Available online 30 May 2017

Keywords:
Polymer electrolyte membrane fuel cell
Oxygen reduction
Catalyst
Ordering
Stability

ABSTRACT

The application of intermetallic compounds in heterogeneous catalysis had a significant boost during the last decade. Notwithstanding the advantages related to the use of intermetallics in catalysis, random alloys, more easy to prepare, are commonly used as catalysts in low temperature polymer electrolyte membrane fuel cells (LT-PEMFC). In various papers, however, the use of Pt- and Pd-based intermetallics in LT-PEMFCs is reported. In this work an overview of the effect of the crystal structure ordering on the activity for oxygen reduction and stability of fuel cell catalysts is discussed, by comparing ordered and disordered structures with the same A/M (A = Pt, Pd; M = first row transition metal) atomic ratio and ordered structures with different A content.

Contents

E-mail address: ermantol@libero.it

http://dx.doi.org/10.1016/j.apcatb.2017.05.081
0926-3373/

1. Introduction

Low temperature acidic fuel cells, fuelled with hydrogen or low molecular weight alcohols consist of an anode, to which the fuel is supplied, a cathode to which oxygen (or air) is supplied, and a polymer electrolyte membrane that permits the flow of protons from anode to cathode [1,2].

Platinum has the highest catalytic activity for oxygen reduction of any of the pure metals, thus unsupported and carbon supported platinum nanoparticles are commonly used as fuel cell electrocatalysts. The oxygen reduction reaction (ORR) electrocatalysis mainly depends on the interplay of electronic and geometric parameters, controlling the adsorption of oxygenated species [3]. Theoretical and experimental studies on the ORR have indicated that Pt–Pt bond compression results in d-band down-shift, weakening the bonding between Pt and oxygenated species and increasing the catalytic activity for the ORR [4,5]. For the ORR intermediates O and OH, this occurs by a simple electron interaction, where the adsorbate valence p-level forms bonding and antibonding states with the metal d-band. [6]. Population of any antibonding state will lead to Pauli repulsion, and the bond strength will thereby be weakened. A downward shift of the d-band will pull more of the antibonding states below the Fermi level, resulting in increasing occupation and weaker adsorbate bonding.

The high cost of platinum and kinetic limitations of the ORR, as well as the low alcohol tolerance when Pt is used as a cathode catalyst in direct alcohol fuel cells, are a major problem for the commercialization of low-temperature fuel cells. So the research focused on the development of cathode catalysts more active, more alcohol-resistant and less expensive than Pt alone, such as binary and ternary Pt-based [7,8] and Pd-based [9] catalysts. The suitability of binary and ternary Pt- and Pd-based catalysts as fuel cell cathode catalysts is mainly based on the fundamental relationship between the electronic surface structure and the ORR activity [10]. Depending on the center of the d-band *vs*. the Fermi level, a direction for development of suitable fuel cell catalysts was traced: highly active ORR catalysts will be obtained by the downshift of the d-band center *vs.* pure Pt, that is, by the weaker interaction of the oxygenated species with the surface [11]. Pt-M and Pt-M-M' (M,M' = first row transition metals) showed higher ORR activities than pure Pt [12,13], retained or enhanced even after removal of the transition metal from the catalyst surface and formation of a Pt rich shell by either naturally under operating conditions or intentionally selective leaching of the non-noble transition metal, due to the electronic (ligand effect) and geometric (strain effect) influence of the alloying element inside the core [14,15].

There are two major types of materials formed by two or more metallic elements, that is, alloys and intermetallics. Alloys, also referred as solid solutions, are random mixtures of metals, in which the elemental crystal structure of one of the constituent elements is adopted. Intermetallics are compounds with a defined stoichiometry and crystal structure, with specific sites assigned for the atoms of each constituent element. In intermetallics the position of two (or more) types of atoms is determined, not random. Such ordering differentiates the intermetallic compound from a "common" alloy. Intermetallics display special magnetic, superconducting and chemical properties, due to their strong internal order and mixed (metallic and covalent/ionic) bonding, which are not present in alloys. Alloys have less negative free energy of formation than intermetallics, resulting in a lower thermal stability, and leading to a surface rearrangement and phase separation. Moreover, random site occupancy of alloys limits the availability of catalyst active sites only to certain regions. Conversely, the regular structure of intermetallics would ensure homogeneity of the active sites.

Recently, the use of intermetallics in various chemical transformations, such as hydrogenation/dehydrogenation, oxidation, and steam reforming, and their advantages over alloys has been surveyed [16,17]. Notwithstanding the advantages related to the use of intermetallics in catalysis, random alloys, more easy to prepare, are commonly used as catalysts in low temperature fuel cells (LT-FCs). In various papers, however, the use of Pt- and Pd-based intermetallics in LT-FCs is reported. Intermetallic compounds can be promising for their use as ORR fuel cell catalysts for two main reasons: 1) unlikely random site occupancy of alloys, in intermetallics the 'good' sites for the ORR are available in whole catalyst surface, and 2) they are more stable thermodynamically and are likely to be less susceptible towards surface rearrangement and phase separation under fuel cell operating conditions than random alloys. In this review the effect of the crystal structure ordering on the ORR activity and stability of fuel cell catalysts is discussed, by comparing ordered (O) and disordered (D) structures with the same A/M (A = Pt, Pd; M = first row transition metal) atomic ratio and ordered structures with different A content.

2. Structure of Pt- and Pd-based binary and ternary alloys and intermetallics

2.1. Binary catalysts

2.1.1. Crystal structure

Generally, Pt-M (M = first row transition metal) compounds present four main crystal structures, that is, a disordered $Pt_{1-x}M_x$ solid solution, and the ordered intermetallic Pt_3M, PtM and PtM_3 intermetallics. The chemically disordered $Pt_{1-x}M_x$ (x = 0–1) alloy has a face-centered cubic (fcc) structure (A1 phase, space group: Fm-3m), in which the Pt and M atoms are randomly distributed in all (0,0,0), (1/2,1/2,0), (1/2,0,1/2) and (0,1/2,1/2) crystallographic sites. $Pt_{1-x}M_c$ alloys order at concentrations x = 1/4 and 3/4. In the ordered fcc Pt_3M structure M atoms occupy the eight corner positions and Pt atoms occupy six-face centered positions in the cube. The structures of Pt_3M and PtM_3 are both $L1_2$, space group: Pm-3m, where the roles of Pt and M are interchanged. Unlike the fcc structure, in the ordered face-centered tetragonal (fct) PtM structure ($L1_0$ phase, space group: P4/mmm) the M and Pt atoms form alternating layers within the crystal lattice, where Pt is in (0,0,0) and (1/2,1/2,0) sites, and M is in (1/2,0,1/2) and (0,1/2,1/2) sites. The fct structure breaks the cubic symmetry of the fcc structure by altering the length of one of the sides. As an example, the crystal structures of the disordered $Pt_{1-x}Fe_x$ solid solution and the fcc Pt_3Fe and fct PtFe ordered phases are shown in Fig. 1 [18]. The fct structure, however, can present a certain degree of disorder, when antisites or antiphases are present. An antisite is formed when some M occupy the (0,0,0) and (1/2,1/2,0) sites and some Pt occupy the (1/2,0,1/2) and (0,1/2,1/2) sites. Vacancies are the other punctual defects present in these intermetallics. If the vacancy concentration is different on both sublattices, a stoichiometry departure will also be induced [19]. Punctual defects in the $L1_0$ structure (antisites and vacancies of both species) are shown in Fig. 2. Antiphase domain boundaries (APBs) are the most common type of extended defects unique to chemically ordered alloys. For example, the unit cell of ordered PtCo with the $L1_0$ structure type is made up of planes of all cobalt and platinum alternating along (002). A scheme of this structure type is shown in Fig. 3a [20] and a representation of the alternate stacking along the c-axis is given in Fig. 3b. The formation of a long-period antiphase structure from $L1_0$ is shown schematically in Fig. 3c. Halfway along the a_1-axis of the cell, the stacking sequence changes in that planes of all cobalt become all platinum and vice versa. Thus, the structure is divided into domains with adjacent domains being antiphase. The antisite defects, vacancy difference and antiphases are responsible in the stoichiometric alloys for the departure of the long-range order parameter from its maxi-

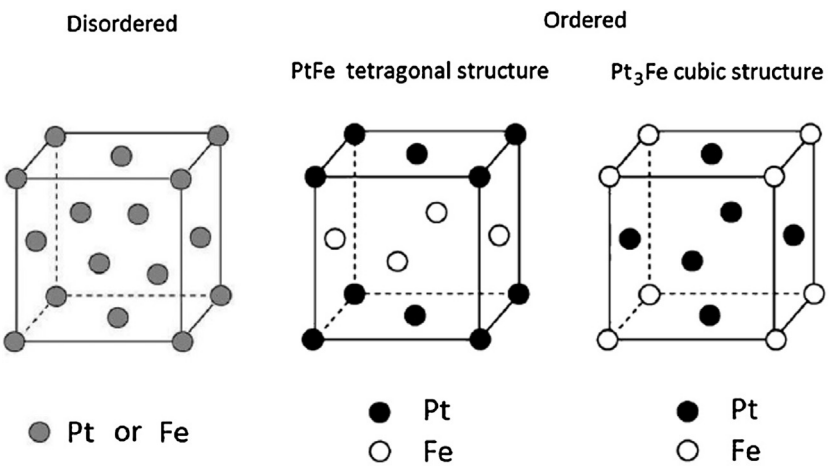

Fig. 1. Crystal structure of disordered Pt_xFey alloys [Fm-3m] and ordered tetragonal PtFe [P4/mmm] and ordered cubic Pt_3Fe [Pm-3m]. Reproduced from Ref. [18], copyright 2012, with permission from Elsevier.

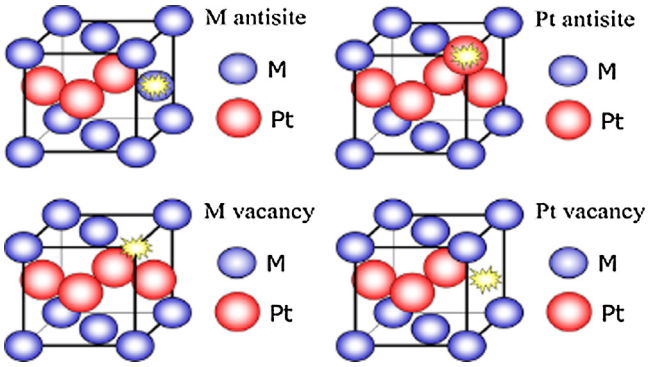

Fig. 2. Punctual defects in the $L1_0$ structure: antisites and vacancies of both species. The defect is emphasized by a flash symbol. Reproduced from Ref. [19], copyright 2015, with permission from Elsevier.

mum value [19]. The ordering parameter S can be determined from the *c/a* axial ratio. S is given by [21]:

$$S^2 = [1-(c/a)]/[1-(c/a)_f] \quad (1)$$

where $(c/a)_f$ is the axial ratio for the fully ordered phase, and (c/a) is for the partially ordered phase. S = 1 in Eq. (1) means the fully ordered phase regardless of composition deviation. For bulk crystals, the degree of ordering decreases with increasing temperature. Nanoparticles, however, being synthesized at room temperature, as the growth kinetics are much faster than the ordering kinetics, are in an almost disordered form. Thus, to transform from the initial disordered to the ordered state, they have to be submitted to an annealing process at high temperature. Endo et al. [22] investigated the structural changes of as prepared Pt-Fe following various annealing temperatures: the ordering parameter increased with increasing thermal treatment temperature. In the temperature range 300–425 °C, the nanoparticles were partially ordered, being S between 0.5–0.75. For temperature above 425 °C, the ordering parameter is approaching 1, indicating a fully ordered phase.

As in the case of platinum, first row transition metals and palladium can form a continuous series of fcc solid solutions and some ordered phases with compositions Pd_3M, PdM or PdM_3 (M = Fe, Co, Ni) [23]. The Pd_3M and PdM_3 phases are in a fcc form, while the PdM phase can be either in a body centered cubic (bcc, B2 phase) or in a fct form.

2.1.2. Surface composition

The surface composition of alloy nanoparticles is generally different from that of the bulk. The driving force for segregation is always thermodynamics, leading to a reduction in the total free energy of the particle [24]. In a random metallic alloy the surface composition is mainly determined by the surface segregation of one of the components, which lowers the surface energy. But for ordered alloys segregation can depend on other factors, that is, most of the surface truncations of a perfectly ordered alloy have a composition different from that of the bulk simply for crystallographic reasons. The simultaneous tendencies of surface segregation and atomic ordering in metallic alloys can be manifested in many ways: long-range order (LRO) can impede segregation in alloys with elemental mixing tendency, or alternatively, strong segregation tendency can disrupt LRO. Conversely, segregation from a disordered bulk can lead to enhanced order at the surface [25]. Ruban [26] predicts the existence of an off-stoichiometric effect in ordered alloys in the form of a distinct transition in the surface segregation behaviour of alloy components near the bulk stoichiometric composition. It is caused by the discontinuity in the effective chemical potential at the stoichiometric composition. The effect is predicted to occur at the (111) surface of ordered Ni_3Al and Pt_3Fe alloys. A simplified 5-layer slab model was used to study Pt segregation at ordered Pt_3M (111) surfaces [27]. To model different Pt_3M crystalline alloys, they assumed that the Pt_3M alloys have fcc structures, in which the Pt atoms occupy the face-centered positions and the M atoms are located at the corners in the unit cell. The segregation structures were obtained by exchanging M atoms at the first layer and Pt atoms at the second layer. In this way, the topmost layer is fully covered by Pt atoms and the second layer contains 50% Pt atoms for each Pt segregation structure. The atoms in the top three layers were allowed to relax to the lowest energy configuration, while the atoms of the bottom two layers were fixed to their bulk positions in keeping with the optimized lattice constants. In general, the surface segregation energy is the energy of moving an atom from the interior to the surface of a crystal, but in this work it is defined as the difference of total free energies of the slab with the Pt segregated structure and that with the bulk structure. A negative segregation energy indicates that the Pt atoms are able to segregate to the surface, while a positive segregation energy suggests no Pt segregation on the surface. Most Pt_3M alloys showed a negative value of the calculated segregation energy, indicating Pt segregation on the surface. Theoretical and experimental works were addressed to Pt segregation on Pt_3Ni and Pt_3Co with Pt segregation [28–31]. Wang et al. [28] reported a theo-

retical approach to predicting surface segregation in nanoparticles by using a modified embedded atom method and Monte Carlo simulations. The results showed that the Pt concentration is nearly 100 at.% in the outermost layer of $Pt_{75}Ni_{25}$ nanoparticles. This theoretical prediction quantitatively agrees with a direct measurement for Pt_3Ni(100), (110), and (111) single crystals [29] and annealed $Pt_{75}Ni_{25}$ polycrystal surfaces [30], in which the Pt concentration in the outermost layer is about 50 at.% higher than in the second atomic layer and the Pt concentration in the third atomic layer is about 75 at%. By aberration-corrected scanning transmission electron microscopy (STEM), STEM image simulations, and density functional theory (DFT) calculations, it was found that acid-leached Pt_3Co nanoparticles exhibit a solid-solution structure but heterogeneous composition, while heat-treated nanoparticles exhibit an ordered structure, except for the first three surface layers where Pt enrichment is observed [31].

2.2. Ternary catalysts

2.2.1. Crystal structure

The same crystal structures reported in the case of binary alloys and intermetallics can be observed in ternary Pt-M_1-M_2 catalysts, in which generally the crystallographic sites occupied by M atoms are now randomly occupied by M_1 or M_2 atoms. In some case, however, the third component can occupy the crystallographic sites occupied by Pt atoms. For example, two different type of fct Pt-Fe-Cu structures were reported, that is, 1) for Pt:(Fe + Cu) compositions = 1:1 Fe atoms are substituted partially by Cu atoms in lattice planes corresponding to the (1/2,0,1/2) and (0,1/2,1/2) crystallographic sites of fct Pt-Fe, while only Pt is present in the (0,0,0) and (1/2,1/2,0) sites [32–34], and 2) for Pt:Fe:Cu compositions = 1-x:1-y:x + y Cu is present in every plane, while the Pt and Fe atoms are present in alternate planes [18].

2.2.2. Surface composition

DFT calculations were used to calculate the Pt surface segregation energy in the Pt_3Ni (111) surface doped with a third transition metal M [35]. Replacing Ni with transition metals V, Fe, Co, Mo, Tc, Ru, W, Re, Os, and Ir resulted in an even more negative Pt surface segregation energies than that in the based Pt_3Ni (111) surface, while replacing Ni with Ti, Cr, Mn, Cu, Zr, Nb, Rh, Hf, and Ta would still retain the preference of Pt segregation to the surface but with less extent than the replaced Ni, and finally Pd, Ag, and Au would completely suppress the Pt surface segregation.

3. Activity and stability of binary A-M (A = Pt, Pd; M = first row transition metal) alloys and intermetallics for the oxygen reduction reaction

The catalytic properties for oxygen reduction of binary platinum alloys were screened using a high throughput combinatorial method [36]. Candidate catalysts were identified by comparing the activity–stability–composition relationships between the platinum alloys and a pure platinum standard. The most promising alloy compositions display ratios of Pt to base metal of either 3:1 (PtCo, PtFe, PtMn, PtTi, PtV, and PtZn) or 1:1 (PtCu, PtMo, PtNi, and PtRe), corresponding to the two ordered structures. A compromise between ORR activity and stability was made to identify the most effective alloys for their use in low-temperature fuel cells. For example, a PtCo alloy with 78 at% Pt and 22 at% Co showed the largest mass-fraction specific activity and a relatively small composition change after stability testing. On this basis, this alloy was identified as the best for the PtCo system. But, notwithstanding the advantages of intermetallics over alloys, research efforts on the development of low-temperature fuel cell catalysts mainly focused on the disordered Pt-M alloys, more easy to prepare, while only few studies were addressed to ordered Pt-M intermetallics. The poor interest in the ordered compounds was also due to their low specific surface area, owing to particle sintering during the high-temperature annealing necessary to obtain ordered phases. Indeed, the mass activity (MA) of a catalyst depends on both its specific activity (SA) and its specific surface area (SSA), as:

$$MA = SA * SSA \quad (2)$$

where SA represents the intrinsic activity of a catalyst surface, while SSA is a measure of the active surface area per unit precious metal mass. In various papers, however, studies on intermetallic compounds, commonly Pt_3M and PtM intermetallics, for a possible use in low-temperature fuel cells are reported. The most part of these studies were addressed to the direct comparison of disordered fcc A_3M and AM_3 with ordered A_3M,and AM_3, and of disordered fcc AM with ordered fct or bcc AM catalysts. Some works focused on the effect of ordering increase in fct AM compounds. It has to be remarked that the obtainment of a fully alloyed disordered cata-

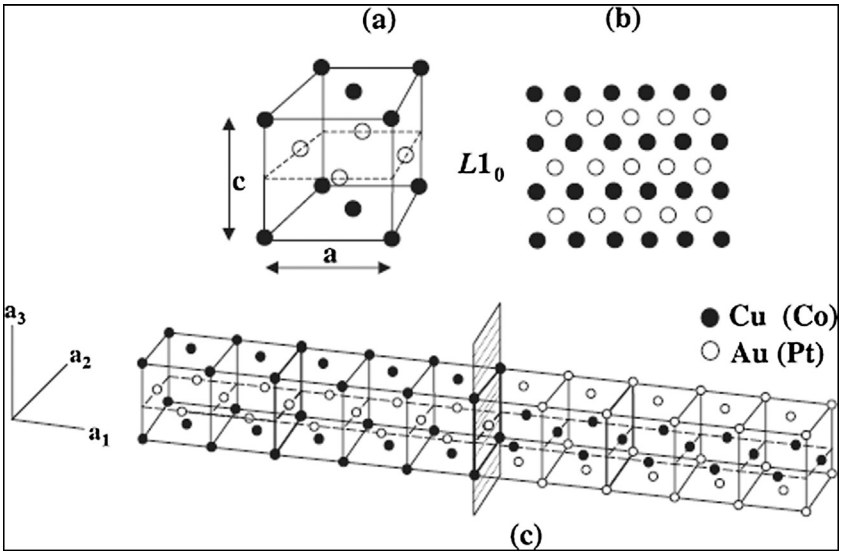

Fig. 3. (a) Scheme of a $L1_0$-type unit cell; (b) alternate stacking of atoms along the c-axis for $L1_0$-type ordered materials; (c) formation of antiphase domains in $L1_0$-type ordered materials. Reproduced from Ref. [20], copyright 2003, with permission from Elsevier.

Table 1
Comparison of the ORR mass and specific activity, measured at the same voltage and temperature, and stability of ordered and disordered Pt_3M (M = Cr, Fe, Co), PtM_3 (M = Cu, Co) and Pd_3Fe catalysts.

Catalyst	SA	MA	Stability	Reference
Pt_3Cr	+	–	+	[38]
Pt_3Cr	+	+	+	[39]
Pt_3Cr	+	–	+	[41]
Pt_3Fe	+	≈	n.d.	[18]
Pt_3Co[a]	+	+	+	[40]
Pt_3Co[b]	+	–	n.d.	[42]
Pd_3Fe	+	+	+	[43]
$PtCu_3$[c,d]	+	+	+	[44]
$PtCu_3$[d]	+	–	n.d.	[46]
$PtCu_3$[d]	+	+	+	[47]
$PtCo_3$[d]	≈	≈	≈	[48]

(+) Activity/stability ordered > activity/stability disordered.
(–) Activity/stability ordered < activity/stability disordered,
(≈)Activity/stability ordered similar activity/stability disordered.
n.d. Not determined.
[a] Pt skin on ordered Pt_3Co.
[b] Ordered PtM_3@Pt/disorderd PtM_3@Pt.
[c] Disordered core-ordered shell/disordered alloy.
[d] Dealloyed catalysts.

lyst, with the same composition of the corresponding intermetallic is not easy. Indeed, generally, random and ordered catalysts are prepared with thermal treatment at lower and higher temperature, respectively. In the synthesis of disordered catalysts, if the annealing temperature is too low, it is possible that part of M in the catalyst is present in an non-alloyed form or that a multiple phase system with different composition is formed, while a heat treatment temperature too high can give rise to the formation of partially ordered catalysts. In these cases, the ordered catalyst is compared with a disordered catalyst with a lower amount of M atoms I the alloy or with a multiphase system or with a partially ordered catalyst.

3.1. *Fcc Pt_3M (M = Cr, Fe, Co), PtM_3 (M = Co, Cu) and Pd_3Fe alloys and intermetallics*

In a pioneering work, Glass and Taylor [37] observed that the atomic ordering in fcc Pt_3Cr catalysts increases the activity for oxygen reduction. Then, a higher specific activity and stability in a acid solution but a lower mass activity of a fully ordered than a partially ordered Pt_3Cr catalyst was reported by Kim et al. [38]. More recently, the ORR mass and specific activities of some ordered fcc intermetallic compounds were compared with that of the corresponding fcc disordered alloys. Pt- and Pd-based alloys and intermetallics with the same non-precious metal were obtained from either the same procedure using the same metal precursors, but thermally treated at different temperature [18,39,40], with the ordered catalysts formed at higher temperature, or the structural transformation upon thermal treatment of the disordered [41–43] (partially ordered [44,45]) compounds in the ordered (disordered) structures. Ordered and disordered PtM_3 core/Pt-shell (PtM_3@Pt) catalysts were also obtained by electrochemical and chemical dealloying of $PtCu_3$, respectively, ($PtCu_3$@Pt) [46], by electrochemical dealloying of $PtCu_4$ catalysts thermally treated at different temperature ($PtCu_3$@Pt) [47], and by chemical dealloying of $PtCo_x$ catalysts with different Co content ($PtCo_3$@Pt) [48]. As can be seen in Table 1, ordered Pt_3M (M = Cr, Fe and Co) [35,40–42] and Pd_3Fe [43] catalysts with (M = Co) or without (M = Cr, Fe) the presence of a Pt-skin showed higher ORR specific activity and stability than the corresponding disordered catalysts. In the same way, ordered PtM_3@Pt (M = Cu,Co) catalysts were more intrinsically active than the corresponding disordered PtM_3@Pt catalysts [44,46–48].

As the intermetallic compounds are generally obtained by thermal treatment at higher temperatures than random alloys, they have a larger particle size, which can affect both SA and MA. The higher specific activity of the ordered catalysts could be ascribed not only to an ordering effect but also to a particle size effect [49]. Indeed, in the case of the ORR, the SA always increases with increasing particle size, up to reach a maximum value, above which the activity is almost constant. Notwithstanding the high specific activity, however, the mass activity of ordered intermetallics was lower or only slightly higher than that of disordered alloys. Indeed, the higher particle size gives rise to a lower electrochemically active surface area (ECSA), resulting in a lowering of the mass activity. For example, Chen et al. [42] obtained an ordered Pt_3Co catalysts by annealing of the disordered Pt_3Co compound. Following thermal treatment, the particle size increased almost twice. As a consequence, the ECSA, obtained from the integration of the surface of the hydrogen adsorption-desorption peak from cyclic voltammetry (Fig. 4a), decreased less than half. Thus, notwithstanding the higher SA of the ordered catalysts than that of the disordered alloy (Fig. 4b), the MA of the Pt_3Co intermetallic was lower than that of the random alloy.

After dealloying, $PtCu_3$@Pt catalysts with ordered core showed higher SA than those with disordered $PtCu_3$ core [44,46,47]. The effect of chemical dealloying on the structural ordering and the active surface area of a $PtCu_3$ catalyst was described by Dutta et al. [50]. Before dealloying in the $PtCu_3$ compound Pt and Cu atoms were arranged in two crystalline forms, that is, a disordered fcc *Fm3m* structure in the composition $Pt_{42}Cu_{58}$ and a partially ordered fcc Pm3m $PtCu_3$ structure. Upon dealloying, however, a significant fraction of the copper was removed to give a material with a Pt/Cu ratio of 1.8. In this case two disordered fcc Fm3m structures in the composition $Pt_{37}Cu_{63}$ and $Pt_{52}Cu_{48}$ were observed. As a consequence, the SA of the $PtCu_3$ catalyst decreased by 1.3 times, owing to the structural ordering decrease, but the MA increased by 2.1 times, as dealloying increased the ECSA. The structural ordering of a dealloyed compound, however, seems to depend on the dealloying method [46]. Indeed, chemical dealloying of an ordered $PtCu_3$ intermetallic compound destroy the ordered structure, resulting in a disordered alloy, while electrochemical dealloying maintain the initial ordered structure. As a consequence, the SA of the chemically dealloyed catalyst was lower than that of the electrochemically dealloyed catalyst, owing to the loss of the ordered structure, while the MA of the chemical dealloyed compound was higher than that of electrochemically dealloyed catalyst, due to the increased surface area resulting from nanovoids formed after chemical leaching. Conversely, notwithstanding the different structure, ordered and disordered $PtCo_3$@Pt obtained by chemical dealloying of carbon supported PtCo and $PtCo_3$ catalysts, respectively, showed similar mass and specific activities and durability [48]. The ordered $PtCo_3$, however, was surrounded by a solid Pt shell, while the disordered $PtCo_3$ core was covered by a porous Pt shell. Likely, the more accessible Pt sites in the porous Pt shell should counterbalance the ordering loss.

3.1.1. *Intrinsic ordering effect on the ORR activity*

ORR electrocatalysis mainly depends on the interplay of electronic and geometric parameters, controlling the adsorption of OH species from the electrolyte at potentials above 0.80 V *vs.* RHE [12]. In the absence of Pt segregation, the dependence of the ORR activity of ordered Pt_3M catalysts on the electronic (Pt d-band vacancies per atom) and geometric parameters (Pt–Pt bond distances) showed a volcano type behaviour, where, among the catalysts investigated, Pt_3Cr/C lies at the top of the curve, presenting the best combination of the Pt d-band vacancies and the Pt–Pt bond distance [12]. Random site occupancy of alloys limits the availability of catalyst active sites only to certain regions. Conversely, the regular structure of intermetallics would ensure homogeneity of the active sites. Regarding the disordered structure, since the Pt and M atoms are

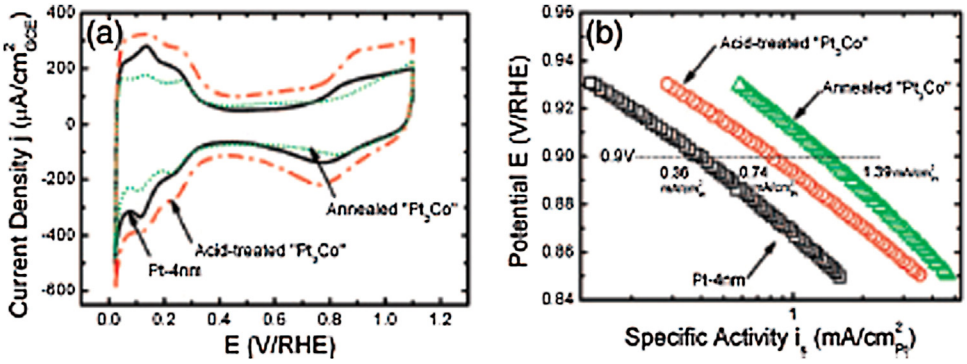

Fig. 4. (a) Cyclic voltammograms of Pt–4 nm, acid-treated, and annealed "Pt_3Co" collected in N_2-saturated 0.1 M $HClO_4$ (room temperature and 50 mV s^{-1}). (b) Tafel plots obtained from polarization curves collected in O_2-saturated 0.1 M $HClO_4$ on a rotating disk electrode in the positive-going scan at 1600 rpm at a sweep rate of 10 mV s^{-1}. Reproduced from Ref. [42], copyright 2008, with permission from The American Chemical Society.

randomly distributed, the M atoms may not be placed in appropriate sites to allow for unperturbed adsorption of OH^- ions. The repulsive force between the OH^- ions during adsorption on adjacent sites can make the adsorption more difficult, leading to a lower coverage of OH^- ions.

Regarding Pt segregation on solid solution and intermetallic surfaces, Pt can segregate in the outermost layer to form either a "Pt-skin structure" with a "Pt sandwich-segregation", typical of ordered structures [30,31] or a "Pt-skeleton structure", proposed for disordered Pt surfaces [51,52]. In the case of Pt-skin on ordered Pt_3M, the enhanced ORR activity was related to the Pt sandwich-segregation structure. Not only can the M-rich layers below the Pt-skin compress the surface Pt–Pt bond distance, but also they can induce the ligand effect due to Pt-M bonds. Combined effects lead to a more reduced reactivity of surface Pt atoms toward oxygenated adsorbates and a more increased ORR activity than the Pt-skeleton structure. Another possibility is that structural ordering changes the lateral strain in the Pt-skin overlayer and hence changes the binding energies of adsorbates [53]. In the case of dealloyed $PtCu_3$@Pt catalysts with identical initial compositions and particle size distributions, the increased ORR activity of the ordered structure with respect to the disordered counterpart was ascribed to a more convenient Pt-Cu coordination, with Pt atoms in the ordered structure surrounded by 15–30% more Cu atoms the in the random alloy [54].

3.1.2. Stability of ordered catalysts

In addition to the previously cited works, an earlier and a more recent study attest to the high resistance to Co dissolution of the ordered Pt_3Co intermetallic compound: early Beard and Ross [55] tested different Pt-Co (3:1) alloys and intermetallics as cathode catalysts in phosphoric acid fuel cells (PAFCs). Post test XRD analyses revealed that, among all the catalysts, the ordered Pt_3Co phase retained the highest amount of Co. The disappearance of superlattice lines and the presence of pure Pt suggested the destruction of the ordered structure and Pt segregation on the catalyst surface, respectively. A similar result was observed by Koh et al. [56]: they synthesized Pt-Co (3:1) electrocatalysts using liquid impregnation techniques followed by reductive annealing at high and low temperatures. Low temperature treatment resulted in a biphasic system, formed by ordered fct and disordered fcc Pt-Co phases, while high temperature annealing resulted in a single ordered fcc Pt_3Co phase. During the electrochemical test, the ordered fct phase showed corrosion, dissolution, preferred Co leaching and particle sintering. The ordered fcc phase of the high temperature catalyst was not a stable structure under electrochemical conditions (the ordered fcc Pt_3Co phase transformed into a disordered fcc Pt_3Co solid solution), but lost only negligible amounts of Co and appeared more resistant to particle sintering compared to the low temperature alloy phases. As the evaluation of the durability of Pt alloys and intermetallics as anode and cathode catalysts directly in low-temperature fuel cells requires much time, accelerated durability tests (ADTs) were developed to evaluate the long-term performance of the Pt alloys, the main ADTS being acid immersion and repetitive potential cycling (RPC). The stability of Pt-based acidic fuel cell catalysts can be considered in two regards: active surface area decrease, due to sintering, and transition metal dissolution under the operating conditions. Generally, the formation of a Pt skin on the surface of Pt_3M alloys and intermetallics hinders the dissolution of bulk Pt and M atoms [41,55,57,58]. In the case of ordered Pt_3M catalysts, the formation of a Pt-skin can occur with [55] or without [41] the structural transformation of the ordered Pt_3M phase to a disordered phase. The high corrosion resistance of the Pt skin formed on the surface of Pt_3M (M = Fe, Co, and Ni) catalysts was explained by Greeley and Norskov by first-principles calculations [59]. They found that the dissolution potential of Pt in Pt "skin" layers from Pt_3M bulk alloys increased by 0.19, 0.16, and 0.14 V for Pt_3Fe, Pt_3Co, and Pt_3Ni, respectively, with respect to the dissolution potential of pure Pt. Thus, the corrosion of Pt_3M alloys and intermetallics with both "Pt-skin" and "Pt-skeleton" structures is believed to be negligible in liquid electrolyte. The higher stability of ordered fcc Pt_3M catalysts compared to disordered ones has to be ascribed not only to an ordering effect, but also to a particle size effect. As previously reported, generally ordered catalysts have a higher particle size than disordered ones. It is well known that the structural stability of carbon supported Pt and Pt-based nanoparticles increases with increasing particle size [60–63]. Small particles possess high surface-area-to-volume ratio, so they tend to grow to lower their surface free energy [64]. Moreover, under potential cycling, Pt particles are subject to a Pt dissolution/re-deposition process [65,66]. Since the atoms at edges and corners on the Pt surface, present in a high content in small particles, are low coordinated, they have strong affinity to oxygenated species generated in the electrode reaction, and they are more inclined to the Pt dissolution process compared to the face atoms. Thus, the higher resistance to sintering of ordered catalysts has to be ascribed to their higher particle size rather than the ordered structure. The structural ordering, instead, affects M dissolution in Pt_3M and PtM_3 catalyst. The better retention of M in ordered fcc Pt_3M and PtM_3 structures has to be ascribed to the fact that in the ordered $L1_2$ phase the average M coordination number of Pt atoms is higher than in the disordered A1 phase. Therefore in disordered samples it is statistically easier to remove M from the alloy since the M-M bonds are weaker than the M-Pt bonds [45].

Table 2
Comparison of ORR specific and mass activities, measured at the same voltage and temperature, and stability of ordered and partially ordered/disordered binary PtM (M = Co, Fe, Ni) and PdCu catalysts and ternary Pt-Fe-M (M = Cu, Co, Ni) compounds. (O/D) disordered fcc-ordered fct(bcc) transition; (OI) ordering increase in the fct phase; (O-D) biphasic disordered fcc- ordered fct(bcc) system.

Catalyst	SA	MA	Stability	Reference
PtCo (O/D)	+	n.d.	–	[67]
PtCo (O/D)	+	+	n.d.	[73]
PtCo (O/D)	n.d.	n.d.	+	[77]
PtCo (OI)	+	n.d.	n.d.	[81]
PtFe (OI)	+	–	n.d.	[18]
PtFe (O/D)	+	n.d.	n.d.	[33]
PtFe (O/D) (OI)	+	+	+	[68]
PtFe (O/D)	+	n.d.	n.d.	[69]
PtFe (O/D)	+	+	+	[70]
PtFe* (O/D)	+	+	+	[72]
PtFe (O-D/D)	+	+	+	[78]
PtFe (OI)	+	n.d.	n.d.	[81]
PtNi (O/D)	+	+	+	[71]
PtNi (O-D/D)	+	n.d.	+	[80]
PdFe[a] (O/D) (OI)	+	+	+	[74]
PdCu (O/D)	+	+	+	[75]
PdCu (O/D)	+	n.d.	+	[76]
PdCu (O-D/D)	+	+	+	[79]
$Pt_{0.92}Fe_{0.92}Cu_{0.16}$ (OI)	+	–	n.d.	[18]
$PtFe_{0.5}Cu_{0.5}$ (OI)	+	+	n.d.	[32]
$PtFe_{0.5}Cu_{0.5}$ (O/D)	+	n.d.	n.d.	[33]
$PtFe_{0.5}Cu_{0.5}$ (O/D)	+	+	n.d.	[34]
$PtFe_{0.5}Co_{0.5}$ (O/D)	+	+	+	[83]
$PtFe_{0.7}Ni_{0.3}$ (O/D)	+	+	n.d.	[84]

(+)/(–) increasing/decreasing activity or stability with increasing ordering.
n.d. = not determined.
[a] Ordered core-Pt shell/disordered alloy.

3.2. Pt_1M_1 (M = Fe, Co, Ni) and Pd_1Cu_1 alloys and intermetallics: disordered fcc to ordered fct or bcc phase transition and ordering increase in the fct crystal structure

In the case of Pt- and Pd-M (1:1) compounds, the transition from a disordered to an ordered phase occurs together with a change in the crystal structure, from a fcc structure to either a fct structure for PtM (M = Fe, Co, Ni) and PdFe catalysts or a bcc structure for PdCu catalysts. In a first work, Watanabe et al. [67] compared the ORR activity and stability of fct ordered and fcc disordered PtCo catalysts. The ordered structure showed a higher SA than the disordered one, but following a corrosion test presented a lower catalytic activity, due to a higher Co dissolution in the ordered catalyst as compared with that in the disordered counterpart. As for the PtCo catalyst, a higher SA of the ordered structures than that of the random alloys was observed in all subsequent works on PtM [33,68–73], PdFe [74] and PdCu [75,76] (Table 2), but the work of Watanabe et al. [67] was the first and only study, reporting a higher stability of a disordered fcc alloy than that of the ordered fct(bcc) counterpart. Indeed, in all subsequent studies, ordered compounds showed a higher corrosion resistance and durability in acid environment than disordered ones [67,70–77] (Table 2). As for A_3M and AM_3 catalysts, also for the AM catalysts, the higher specific activity of the ordered than that of disordered catalysts could be in part ascribed to a particle size effect, due to the increase of particle size during the disordered-ordered transition by thermal treatment at high temperature. Indeed, the main way to obtain ordered AM structures is the fcc to fct(bcc) phase transition by heat treatment at high temperature. Notwithstanding the higher particle size, the MA of ordered fct PtM and bcc PdM catalysts, unlikely from ordered fcc Pt_3M, Pd_3M and PtM_3 catalysts, is generally higher than that of disordered catalysts (Table 2): this depends on the high ordered/disordered specific activity ratio (SA_O/SA_D), which exceeds the decrease in the ECSA. Indeed, as can be seen in Table 3 and Fig. 5, the averaged SA_O/SA_D ratio of AM catalysts is higher than that of both A_3M and AM_3. The higher SA_O/SA_D value for the AM catalysts should be due to the change in the crystal structure occurring together with the ordering increase, while in the case of the fcc A_3M and AM_3 catalyst the fcc crystal structure is preserved.

Table 3
Ratio of specific activity of ordered catalysts divided by that of disordered catalysts in the same composition (SA_O/SA_D), measured at the same voltage and temperature.

Catalyst	SA_O/SA_D	Reference
Pt_3Fe	1.3	[18]
Pt_3Cr	1.5	[39]
Pt_3Cr	1.6	[41]
Pt_3Co	1.9	[42]
Pd_3Fe	2.4	[43]
PtCo	1.4	[67]
PtCo	3.0	[73]
PtNi	3.2	[71]
PtFe	2.4	[33]
PtFe	3.3	[68]
PtFe	2.2	[70]
PdCu	3.0	[79]
PdFe	3.3	[74]
$PtFe_{0.5}Cu_{0.5}$	2.4	[33]
$PtCu_3$[a]	1.4	[44]
$PtCu_3$	1.4	[46]
$PtCu_3$	2.0	[47]
$PtCo_3$	1.0	[48]

[a] (O-D/D).

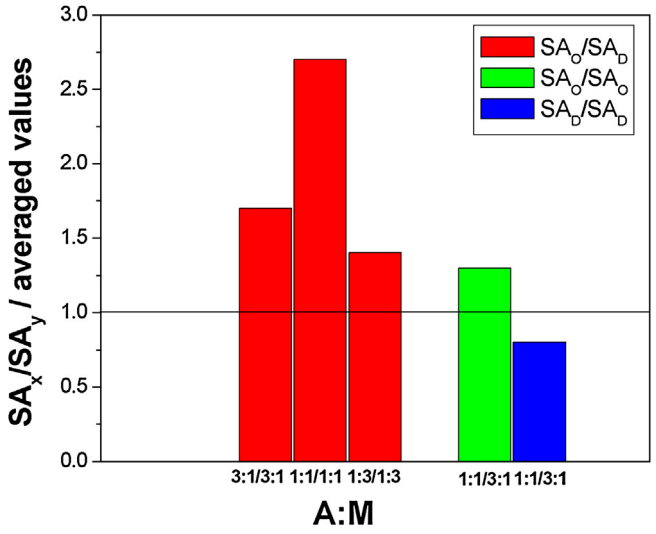

Fig. 5. Averaged SA_x/SA_y ratio for A_3M, AM_3 and AM (A = Pt, Pd; M = first row transition metal) catalysts. (O) = ordered, (D) = disordered. Red bars: x = O, y = D; green bar: x = O, y = O; blue bar: x = D, y = D. (For interpretation of the references to color in this figure legend, the reader is referred to the web version of the article.).

In some cases the fcc → fct phase transition was not complete, thus fcc alloys were compared to a mixture of disordered fcc and ordered fct PtM phases [78–80]. A higher activity and stability of the fcc/fct mixture than those of fcc was always observed, confirming the results of the direct fcc-fct comparison. Moreover, the transition from fcc to fct may lead to the formation of a partially ordered fct phase, depending to transition temperature [18,32,70,81], due to the presence of antisites and/or vacancies. For example, in the case of PtFe, after heat treatment at 600 °C in a sub-lattice normally occupied by Pt atoms (100% in fully ordered PtFe), Pt atoms occupy only 55% of sites, while Fe atoms occupies 45% of sites. Following thermal treatment at 800 °C, instead, the amount of sites occupied by Pt atoms increases to 92%, with Fe atoms occupying the remaining 8% [18]. In all cases, the catalytic activity of partially ordered catalysts increased with increasing the chemical order. The increase of the ORR specific activity and stability (expressed in terms of

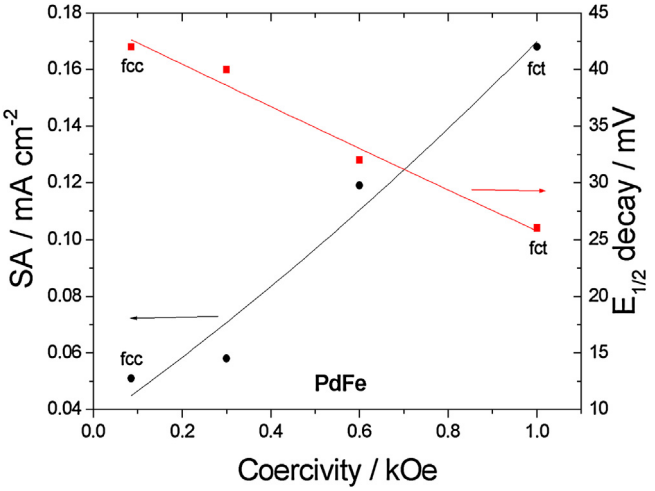

Fig. 6. Dependence of the ORR specific activity and stability (expressed in terms of $E_{1/2}$ decay) with ordering increase (expressed in terms of coercivity increase) for PdFe catalysts.

$E_{1/2}$ decay) with ordering increase (expressed in terms of coercivity increase) for PdFe catalysts is shown in Fig. 6, obtained from data in ref. [74].

3.2.1. *Intrinsic ordering effect on the ORR activity*

The higher ORR activity of ordered fct catalysts than the disordered ones was ascribed to both geometric and electronic effects [33,75,78,82]. Kim et al. [78] attributed the higher activity of the ordered fct than the random fcc PtFe alloy to the intermetallic structure present in the fct PtFe, which offers some ideal catalytic facets around each particle, with Pt sitting on the top and Fe lying under the Pt layer, an essential structural characteristics for an improved catalytic activity. Zhang et al. [33] performed quantum mechanics/molecular mechanics (QM−MM) simulations to calculate Pt−O binding energies (ΔE_O) on the surface of PtFe@Pt particles, formed by either a disordered (fcc-PtFe) or an ordered (fct-PtFe) core and fcc-Pt shell (three atomic layers) The resulting ΔE_O values of the fcc-PtFe@Pt and fct-PtFe@Pt were 0.26 and 0.23 eV, respectively. As the ΔE_O value of the fct-PtFe@Pt was closer to the optimal value of 0.20 eV, it was inferred that the fct-PtFe@Pt has higher ORR activity than the fcc-PtFe@Pt. In a similar way, to explain the dependence of the ORR activity on the structural order of PdCu catalysts, Jiang et al. [75] calculated ΔE_O at the hollow sites of the (111) surface by DFT calculations. For convenience, the optimal ΔE_O was shifted to 0 eV, thus ΔE_O represented the difference of a given ΔE_O value relative to this optimal reference. The distribution of ΔE_O for the disordered PdCu presented a peak at *ca.* 0.2 eV. For the intermetallic PdCu, there were two inequivalent oxygen adsorption sites, whose ΔE_O values were *ca.* 0.2 eV and 0.1 eV. Thus, the average ΔE_O of the ordered alloy was closer to the zero than that of the disordered alloy, suggesting that the former possess higher ORR activity than the latter. To understand the origin of the ORR activity enhancement of ordered PtCo catalysts, Lebedeva et al. [82] carried out spin-polarized electronic structure calculations The polarization leads to the emergence of new unoccupied d states above the Fermi level and to a strong depletion of the density of states at the Fermi level. These effects are more pronounced for the $L1_0$ than for the A1 structure. While the differences in the d-band center between $L1_0$ and A1 structure are relatively small, the width of the d-band for the ordered configuration is much smaller than for the disordered one. The narrowest d-band is indeed obtained when the number of Pt–Pt bonds is minimized, as in the case of the ordered structure, where the Pt surface layer lies onto a pure Co plane. Strain is also a factor affecting the d-band position and the bandwidth, tensile strain leading to the band narrowing, while compressive strain leading to the band broadening. Pt monolayer on a $L1_0$ ordered substrate (Pt–Pt istance of 0.276 nm) is much less contracted than the disordered state (Pt–Pt distance of 0.268 nm). Thus, $L1_0$ structure offers an unique possibility to maximize the favourable electronic influence of Co without an excessive contraction of the Pt lattice.

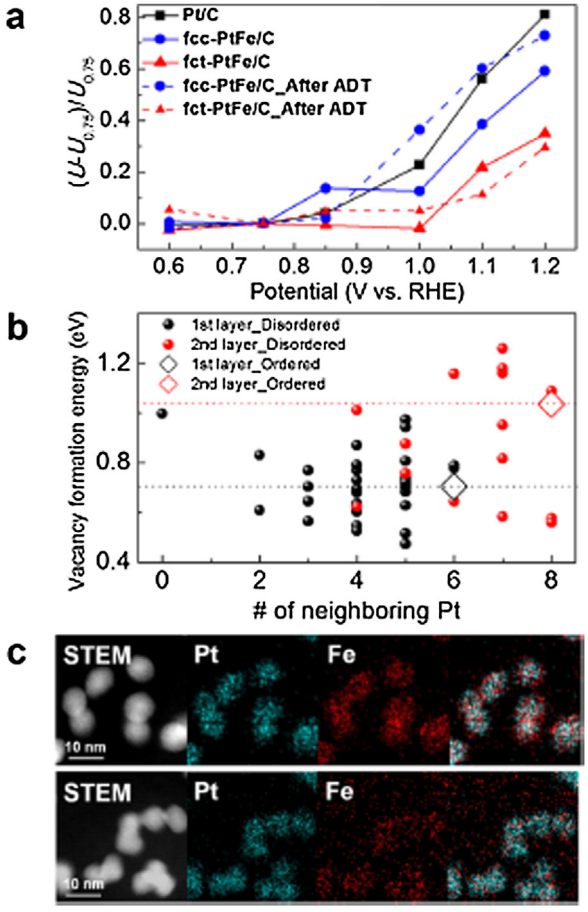

Fig. 7. Long-term stability analysis through in situ XANES, computational analysis, and TEM. (a) Change in the whiteline intensity of the Pt L3-edge as functions of potential measured by in situ XANES analysis. U and $U_{0.75}$ indicate the integrated whiteline intensity and the value of U at 0.75 V, respectively. (b) Vacancy formation energy (E_{vac}) of Fe calculated by first-principles calculations. The dashed lines indicate the values of E_{vac} for the first and the second layers of an ordered fct-PtFe structure. (c) HAADF-STEM and EDS elemental mapping analysis of ordered fct-PtFe/C (up) and disordered fcc-PtFe/C (down) after ADT 10,000 cycles. Reproduced from Ref. [70], copyright 2015, with permission from The American Chemical Society.

3.2.2. *Stability of ordered catalysts*

As we will see in the next section, the structural stability of ordered fct PtM catalysts is not high, but they are more stable than the disordered ones. As for Pt_3M catalysts, the higher stability of ordered fct PtM intermetallics than random alloys has to be ascribed not only to an ordering effect, but also to a particle size effect. To evaluate the ordering effect on the durability, Chung et al. [70] carried out XANES measurements on the Pt L3-edge of ordered fct PtFe/C, disordered fcc PtFe/C, and Pt/C. The extent of Pt oxidation is obtained by the whiteline intensity of XANES spectrum, reflecting the amount of Pt d-band vacancies as a function of potential (Fig. 7a). The oxidation of Pt atoms is one of the major deactivation mechanisms of fuel cell catalysts. From x-ray absorption near edge structure (XANES) measurements it was found that the ordered fct PtFe/C catalyst is more oxidation-resistant than the other two samples. In particular, comparing the PtFe/C samples measured after

ADT, the extent of Pt oxidation of ordered fct PtFe/C is less than half of that of disordered fcc PtFe/C. Considering that Pt atoms of Pt-Fe compounds become easier to be oxidized as more Fe atoms are dissolved from the alloy during ADT, it results that Fe atoms in ordered fct PtFe structure are more stable and less dissolved than those in disordered fcc PtFe. The different stability of Fe atoms in ordered fct and disordered fcc structures was tested by first-principles calculations, and the results are shown in Fig. 7b. The vacancy formation energy (E_{vac}) was calculated for Fe atoms in the first and the second layer at the surface of PtFe catalysts. In the ordered fct structure, E_{vac} of Fe was 0.71 and 1.03 eV in the first and the second layer, respectively, whereas in the disordered fcc structure, E_{vac} had broad distribution due to random arrangement of atoms. As *ca.* half of the values of E_{vac} in both the first and the second layers of disordered fcc structure are lower than 0.71 and 1.03 eV, respectively, it is easier to remove some of Fe atoms from the surface of disordered fcc PtFe than ordered fct PtFe. Moreover, the higher dissolution resistance of Fe atoms in ordered fct PtFe was confirmed by energy dispersive spectroscopy (EDS) analysis of the samples after 10,000 ADT cycles (Fig. 7c). The elemental mapping images of Pt and Fe match well to scanning transmission electron microscopy (STEM) image of ordered fct PtFe, indicating stable PtFe intermetallic structure of the NPs. Conversely, for disordered fcc PtFe, the mapping image of Fe has poor resemblance to either Pt mapping or STEM images. The atomic ratios of Pt and Fe from EDS data show that the amount of Fe in disordered fcc PtFe is significantly decreased from Pt:Fe = 51:49 to 90:10 after ADT, while the change in the atomic ratio of ordered fct PtFe is only from 51:49 to 58:42.

4. Ordered ternary catalysts for the oxygen reduction reaction: comparison with the corresponding disordered ternary and ordered binary catalysts

To aim to improve their activity for oxygen reduction and stability, a third metal was added to binary intermetallics, in particular to Pt-Fe. Ordered ternary Pt-Fe-M (M = Cu, Ni, Co) catalysts were investigated, overall in the fct structure [18,32–34,83–85] and the Pt:Fe:M atomic composition of 1:0.5:0.5 [32–34,83–85] (same Fe and M content), but also in the 0.92:0.92:0.16 [18] and 1:0.7:0.3 [84] compositions (low M content). The fct Pt-Fe-Cu catalysts were the most studied [18,32–34]. As shown in Table 2, the SA and MA of all the ordered ternary fct Pt-Fe-M catalysts were higher than those of fcc disordered catalysts in the same composition. To evaluate the best chemical composition, the dependence of the ORR activity of ordered fct intermetallics (Pt-Fe-M, M = Cu, Ni) on the Fe/M atomic ratio at Pt/(Fe + M) ≈ 1 was investigated [33,84]. The $Pt_1(FeCu)_1$ compounds showed a Cu-dependent fcc–fct transition. [33]. At 650 °C, both $Pt_{47}Fe_{38}Cu_{15}$ and $Pt_{52}Fe_{25}Cu_{23}$ particles showed better fcc–fct transition than the $Pt_{46}Fe_{19}Cu_{35}$ particles, indicating that the presence of too much Cu prevents the formation of the fct structure. Among $Pt_{47}Fe_{38}Cu_{15}$ and $Pt_{52}Fe_{25}Cu_{23}$, the $Pt_{52}Fe_{25}Cu_{23}$ catalyst showed the highest ORR activity. Conversely, the mass activity of $Pt_{50}Fe_{35}Ni_{15}$ was higher than that of fct-$Pt_{50}Fe_{25}Ni_{25}$ and fct-$Pt_{50}Fe_{15}Ni_{35}$, that is, the ORR activity of $Pt_1(FeNi)_1$ increased with increasing Fe content [84]. A direct comparison of the ORR activity and stability of ordered ternary Pt-Fe-M catalysts with the ordered binary PtFe parent was made only in few works, and a little difference was observed: the SA of $PtFe_{0.5}Cu_{0.5}$ was slightly higher ($SA_O^{PtFeCu}/SA_O^{PtFe}$ *ca.* 1.2) [18,33,34], but the SA of $PtFe_{0.5}Co_{0.5}$ was slightly lower ($SA_O^{PtFeCo}/SA_O^{PtFe}$ = 0.9) [34] than that of fct PtFe. The higher ORR activity of fct $PtFe_{0.5}Cu_{0.5}$@Pt than that of fct PtFe@Pt was explained by using QM-MM simulations [33]. The QM–MM simulations on fct $PtFe_{0.5}Cu_{0.5}$@Pt demonstrated that the partial substitution of Fe with Cu in PtFe could further reduce the overcompression on the Pt shell compared to fct PtFe@Pt. As a result, ΔE_O of the fct $PtFe_{0.5}Cu_{0.5}$@Pt was reduced from 0.23 to 0.22 eV. This optimized ΔE_O is predicted to give the fct $PtFe_{0.5}Cu_{0.5}$@Pt the balanced energetics for the adsorption and desorption of oxygenated intermediates, enhancing the ORR activity.

Table 4
Ratio of specific and mass activities and stability of ordered PtM ($PtM_{0.5}M'_{0.5}$) catalysts divided by those of ordered Pt_3M ($Pt_3M_{0.5}M'_{0.5}$) catalysts.

System	SA_O^{11}/SA_O^{31}	MA_O^{11}/MA_O^{31}	Stability	Reference
Pt-Fe	1.1	1.1	n.d.	[18]
Pt-Fe	1.1	1.4	–	[87]
Pt-Fe	1.6	1.7	n.d.	[88]
Pt-Co[a]	1.6	n.d.	–	[56]
Pt-Fe-Cu	1.1	0.8	n.d.	[89]
Pt-Fe-Co	n.d.	1.9	–	[85]

(–) stability (1:1) < stability (3:1).
[a] $fccPt_{95}Co_5$ + fctPtCo/$fccPt_3Co$.

A higher stability of ordered ternary $PtFe_{0.5}Cu_{0.5}$ catalysts that of PtFe was observed [33,34]. The intermetallic fct $PtFe_{0.5}Cu_{0.5}$ catalyst retained more than 70% of its MA and ECSA over 10,000 durability cycles performed at 60 °C [34]. Conversely, the ordered fct PtFe catalyst maintained only about 40% of activity. Over 10,000 durability cycles, the ordered fct $PtFe_{0.5}Cu_{0.5}$ catalyst showed a low Fe and Cu dissolution from the catalyst (25 and 30% decrease in the Fe/Pt and Cu/Pt ratios, respectively), and preserved the maximum extent of the ordered structure. Conversely, a large dissolution of Fe (78% decrease in the Fe/Pt ratio) was identified in the intermetallic fct PtFe catalyst, causing the destruction of the ordered structure. After 5 K durability cycles at room temperature, the intermetallic fct $PtFe_{0.5}Co_{0.5}$ catalyst preserved most of the ordered structure, despite the loss in the average ratios of Fe/Pt and Co/Pt was 50% and 45%, respectively [85]. As the dissolution of a metal from an alloy depends on the standard redox potential, the enhanced durability of the ordered fct $PtFe_{0.5}Cu_{0.5}$ catalyst was explained by the different standard redox potentials of Fe and Cu [34]. The standard redox potentials of the Fe, Cu, and Pt are −0.44 V, 0.34 V, and 1.19 V, respectively, meaning that Fe undergoes oxidation more easily than Cu and Pt. Considering that a metal with a higher standard redox potential can inhibit the dissolution of a metal a lower redox potential, the presence of Cu could reduce Fe dissolution [34].

The stability the ordered $PtCu_3$ catalyst increased by Au addition [45]. In the presence of Au, Cu corrosion is reduced with respect to the $PtCu_3$ ordered catalyst alone. The stabilization effect of Au atoms was predicted by DFT calculations, which showed that subsurface Au increased the energetic barrier to the segregation loss from Pt_3M bulk region [86]. On the other hand, superficial Au is also able to prevent copper dealloying, due to the much faster surface mobility, that is, a passivation ability.

The disordered fcc $PtFe_{0.5}Cu_{0.5}$/disordered fcc PtFe SA ratio ($SA_D^{PtFeCu}/SA_D^{PtFe}$ = 1.4) was similar to that of the ordered fct $PtFe_{0.5}Cu_{0.5}$/ordered fct PtFe ($SA_O^{PtFeCu}/SA_O^{PtFe}$ = 1.2) [33], that is, substantially the addition of Cu has the same effect on the SA of ordered and disordered PtFe catalysts. This is an interesting results: indeed, considering that disordered ternary catalysts for the ORR were widely studied [13], the best ternary catalyst compositions observed in disordered form should be also tested in the ordered form.

5. Comparison of ordered fcc Pt_3M and $Pt_3Fe_{0.5}M_{0.5}$ catalysts with ordered fct PtM and $PtFe_{0.5}M_{0.5}$ catalysts: effect of crystal structure and Pt content

The ORR activity and stability of ordered fcc Pt_3M and $Pt_3Fe_{0.5}M_{0.5}$ catalysts were compared to those of fct PtM and $PtFe_{0.5}M_{0.5}$ catalysts in some works [18,56,85,87–89]. As can be seen in Table 4, where the values of ordered PtM ($PtFe_{0.5}M_{0.5}$) SA

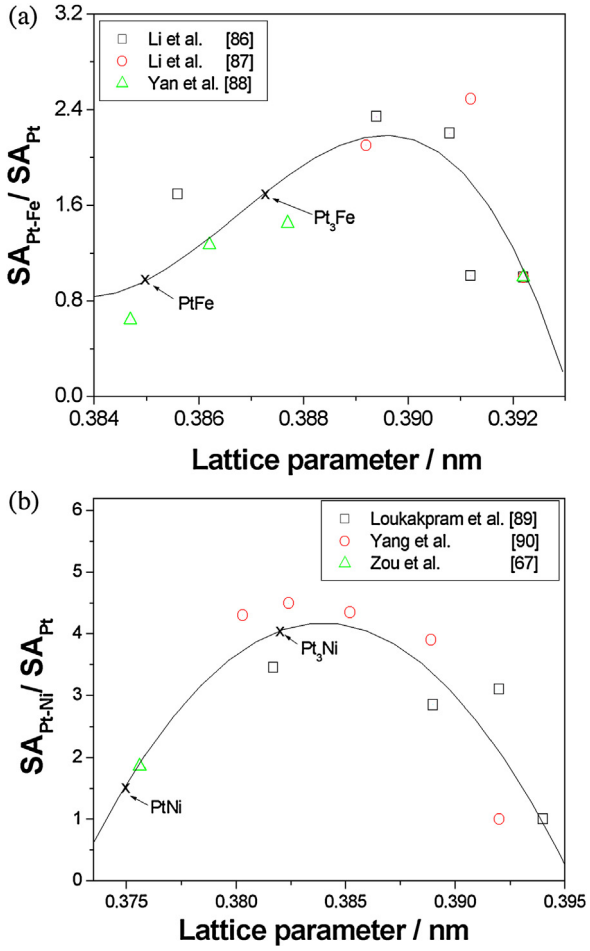

Fig. 8. Dependence of the Pt-M to Pt ORR specific activity ratio ($SA_{Pt\text{-}M}/SA_{Pt}$), with M = Fe (Fig. 8a obtained from data in refs. [90–92]) and Ni (Fig. 8b obtained from data in refs. [71,93,94]), on the fcc lattice parameter.

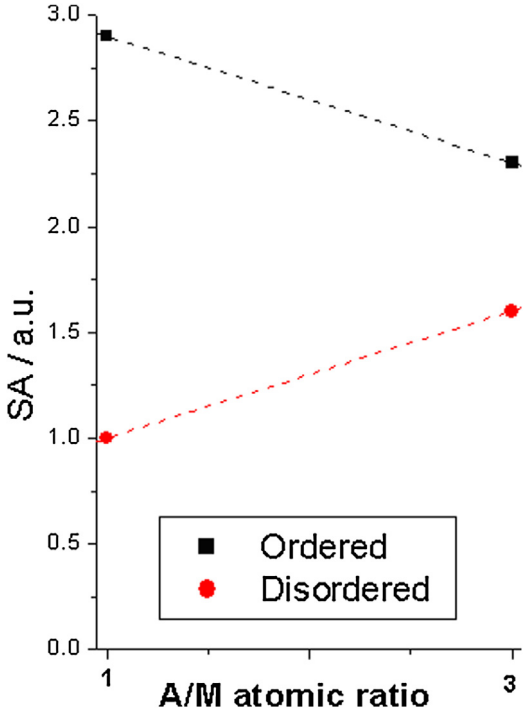

Fig. 9. Dependence of the SA of ordered and disordered A-M (A = Pt, Pd; M = first row transition metal) catalysts on the A/M ratio.

to ordered Pt_3M ($Pt_3Fe_{0.5}M_{0.5}$) SA ratio ($SA_O{}^{11}/SA_O{}^{31}$) of the different catalysts are reported, the SA and MA of fct PtM ($PtFe_{0.5}M_{0.5}$) catalysts were slightly higher than that of ordered fcc Pt_3M ($Pt_3Fe_{0.5}M_{0.5}$) catalysts. Li et al. [87] ascribed the higher activity of ordered fct PtFe than that of ordered fcc Pt_3Fe to both a more suitable distance between the nearest-neighbour Pt atoms (0.274 nm for intermetallic Pt_3Fe and 0.271 nm for intermetallic PtFe and a higher Pt(0) content in PtFe than in Pt_3Fe. Conversely, as can be seen in Fig. 8, where the Pt-M to Pt ORR specific activity ratio ($SA_{Pt\text{-}M}/SA_{Pt}$), with M = Fe (Fig. 8a obtained from data in refs. [90–92]) and Ni (Fig. 8b obtained from data in refs. [71,93,94]), was plotted against the fcc lattice parameter, the SA of disordered Pt_3Fe and Pt_3Ni catalysts was higher than that of disordered PtFe and PtNi samples, respectively. An averaged value of the disordered AM SA to disordered A_3M SA ratio ($SA_D{}^{11}/SA_D{}^{31}$) can be obtained by the average values of SA_O/SA_D for A:M 3:1 ($(SA_O/SA_D)_{31} = 1.7$) and A:M 1:1 ($(SA_O/SA_D)_{11} = 2.7$) from the data in Table 3 and the average value of $SA_O{}^{11}/SA_O{}^{31}$ (1.3) from the data in Table 4 as the following equation:

$$SA_D{}^{11}/SA_D{}^{31} = SA_O{}^{11}/SA_O{}^{31} * (SA_O/SA_D)_{31}/(SA_O/SA_D)_{11} \quad (3)$$

The obtained average value of $SA_D{}^{11}/SA_D{}^{31}$ was 0.8, confirming that the SA of disordered AM catalysts is lower than that of disordered A_3M samples. The histogram of the averaged values of SA_O/SA_D for A:M = 3:1, 1:1 and 1:3, $SA_O{}^{11}/SA_O{}^{31}$ and $SA_D{}^{11}/SA_D{}^{31}$ is shown in Fig. 5: the higher value of the SA_O/SA_D ratio of the catalysts with A:M = 1:1 than that of the catalysts with A:M = 3:1 is due the $SA_O{}^{11}/SA_O{}^{31}$ ratio >1 and the $SA_D{}^{11}/SA_D{}^{31}$ ratio <1. As shown in Fig. 9, where, on the basis of the data reported in Tabs. 1–4, the SA of ordered and disordered A-M catalysts is plotted against the A/M ratio, the SA of ordered catalysts is always higher than that of the disordered ones, but the dependence of the SA on the A/M ratio changes going from random to ordered structures: with increasing noble metal content, the SA of disordered samples increases, whereas a decrease of SA is observed for ordered catalysts. The SA enhancement of the ordered structure with decreasing A content should be ascribed to the structural change from fcc to fct, which is not the case in random catalysts.

Some works attested for a higher stability of ordered Pt_3M and $Pt_3Fe_{0.5}M_{0.5}$ catalysts compared to the ordered PtM and $PtFe_{0.5}M_{0.5}$ ones [56,85,87]. After ADTs, the ordered Pt_3Fe/C showed a reduction in the ECSA value of 3% after 1000 cycles and 30% after 5000 cycles, while the ordered PtFe/C showed an increase in ECSA of 16% after 1000 cycles and 3% after 5000 cycles [83]. The increase in the ECSA of PtFe/C was due to the leaching of Fe, leading to the destruction of the ordered structure. After 5000 cycles, although PtFe/C presented a slight better mass activity than Pt_3Fe/C and Pt/C, due to the ECSA increase, the specific activity of PtFe/C was lower than that of Pt_3Fe/C, and decreased to a value near to that of commercial Pt/C. Ex situ XRD results reveal that after 5000 potential cycles, the PtFe/C electrocatalyst existed as a mixture of two phases, that is, Pt and intermetallic PtFe [87]. A similar result was observed by Tamaki et al. [85] for the $Pt_3Fe_{0.5}Co_{0.5}$ and $PtFe_{0.5}Co_{0.5}$ catalysts: after ADT, the fct $PtFe_{0.5}Co_{0.5}$ catalyst showed an increase of the ECSA, but a higher leaching of both Fe and Co atoms than the $Pt_3Fe_{0.5}Co_{0.5}$ catalyst, also if both catalysts maintained the ordered structure. The SA of $Pt_3Fe_{0.5}Co_{0.5}$ was stable, while that of $PtFe_{0.5}Co_{0.5}$ was 37% lower than that before ADT. Analysis before/after the electrochemical test of a biphasic fcc $Pt_{95}Co_5$/fct PtCo system indicated the stability of the $Pt_{95}Co_5$ phase, but the Co leaching of the ordered fct PtCo phase [56]. Particle sintering occurred for both phases under electrochemical conditions. On the other hand, the ordered fcc Pt_3Co transformed into a disordered fcc Pt_3Co alloy, indicating that the

ordered cubic phase is not a stable atomic arrangement under electrochemical conditions, but it loses only negligible amounts of Co and appears more resistant to particle sintering compared to fct PtCo phase [56]. All these results can be explained by the formation a stable Pt-skin on the catalysts with the higher Pt content. As in the case of ordered catalysts, disordered Pt_3Ni [95], Pt_3Co [95] and Pt_3Cr [39] were more stable than disordered PtNi, PtCo and PtCr, respectively. The stability of disordered fcc Pt-Fe catalysts was evaluated by potential cycling tests [96,97]. Zhang et al. [96] observed a remarkable increase in ECSA of Pt-Fe/C (1:1) within the first 150 cycles, a small ECSA increase at around 50 cycles for the Pt-Fe/C (2:1), and no increase for the Pt-Fe/C (3:1). A similar trend was observed by Malheiro et al. [97], thus highlighting the dependence of the increase of the active area on iron content. After the reaching of the peak, for the $Pt_{1-x}Fe_x$ catalysts with $x < 0.5$ the ECSA of Pt-Fe/C catalysts decreased more slowly than pure Pt with cycling, reflecting the rearrangement of the remaining Pt layer and the formation of a Pt skin layer, protecting the underlying bulk alloy from Fe leaching. On the other hand, the Pt-Fe/C (1:1) catalyst showed a similar decrease of the ECSA than Pt/C, indicating no formation of a stable Pt skin. Over potential cycling, in addition to a higher ECSA stability, the disordered Pt_3Fe catalysts showed a higher stability of the ORR activity than the disordered PtFe ones. Considering that both disordered Pt_3M and PtM catalysts present the same fcc crystalline structure, the higher stability of Pt_3M than PtM catalysts has to be ascribed to the higher Pt content.

6. Conclusions

By comparison of the specific activity for the ORR of ordered and disordered A_3M, AM_3 and AM (A = Pt, Pd; M = first row transition metal) catalysts, it resulted that the SA of the ordered structures is always higher than that of the disordered ones. The structural ordering affects the dependence of the specific activity on precious metal content, that is, with increasing the A/M atomic ratio from 1 to 3 A/M, a decrease of the SA for ordered catalysts, but an SA increase for the disordered ones was observed. The averaged SA_O/SA_D ratios of A_3M and AM_3 catalysts were *ca.* 1.7 and 1.4, respectively, while that of AM system was *ca.* 2.7, so a higher positive ordering effect occurred in AM catalysts, perhaps due to the change in the crystal structure from fcc to fct(bcc). As the intermetallic compounds are generally obtained by thermal treatment at higher temperatures than random alloys, they have a larger particle size, which can affect both SA and MA. The higher specific activity of the ordered catalysts could be ascribed not only to an ordering effect but also to a particle size effect. Indeed, in the case of the ORR, the SA always increases with increasing particle size, up to reach a maximum value, above which the activity is almost constant. On the other hand, the larger particle size of the ordered catalysts gives rise to a lower electrochemically active surface area, resulting in a lowering of the mass activity. As a consequence, notwithstanding the high specific activity, the mass activity of ordered A_3M and AM_3 intermetallics was lower or only slightly higher than that of disordered alloys. In the case of AM catalysts, instead, notwithstanding the larger particle size, the MA of ordered fct PtM and bcc PdM was generally higher than that of disordered catalysts: this depends on the high ordered/disordered specific activity ratio (SA_O/SA_D), which counterbalances the decrease in the ECSA. To increase the mass activity of ordered catalysts, future work should be addressed to the development of low temperature synthesis methods, to obtain small particle size. A way to avoid the sintering problem during high temperature annealing to obtain ordered structures is the coating the disordered catalysts with MgO. By thermal treatment of MgO-coated fcc PtFe catalysts, fct PtFe catalysts with small particle size are obtained, but they are only partially ordered [80]. When the fcc PtFe particles are embedded in the MgO matrix, the Fe, Pt mobility is limited during the annealing and complete structure transition to fct-PtFe is difficult to achieve [98]. To overcome this problem, MgO-coated dumbbell-like fcc PtFe-Fe_3O_4 particles were used as starting material: fcc PtFe/Fe_3O_4/MgO particles were transformed into fct PtFe/MgO particles upon reductive annealing. Hydrogen reduces Fe_3O_4 to Fe, releasing H_2O and causing defects in oxygen sites. Such defects may promote interdiffusion between Fe and Pt-rich PtFe matrix, facilitating the formation of fct PtFe [68].

Regarding the stability, as the order in intermetallic phases arises from the high enthalpy of mixing, a higher chemical and structural stability than in the random ones has to be expected [99]. In agreement with the high enthalpy of mixing, the stability of A_3M, AM_3 and AM ordered catalysts was higher than the disordered counterparts. The higher stability of the ordered catalysts, in particular the higher resistance to sintering, however, could be also due to their larger particle size. Ordered fcc A_3M catalysts showed higher stability than ordered fcc(bcc) AM compounds: this result could be ascribed to both the higher Pt content or a higher stability of the fcc structure than the fct(bcc) structure. But also disordered fcc A_3M catalysts presented a higher stability than disordered fcc AM catalysts. As disordered A_3M and AM catalysts have the same structure, it results that the higher stability of A_3M catalysts than that of AM ones is due to the higher Pt content, which allows the formation of a stable Pt skin.

Among alloys and intermetallics, the ordered A_3M structure seems the most appropriate for the use as ORR catalyst in low-temperature fuel cells, being more active than disordered A_3M and more stable than ordered AM catalysts. Ordered ternary catalysts showed a slight change in the SA, but high stability than ordered binary parents. On this basis, the future direction should be the addition of a third element to ordered AM catalysts to improve their stability, maintaining their high activity, or to add a third metal to ordered A_3M catalysts to improve their ORR activity, maintaining their high stability. Further increase of the specific activity could be obtained by tuning the M/M' ratio, in ordered ternary $AM_xM'_y$ and $A_3M_xM'_y$ catalysts.

The disordered fcc PtFeCu/disordered fcc PtFe SA ratio ($SA_D{}^{PtFeCu}/SA_D{}^{PtFe} = 1.4$) was similar to the $SA_O{}^{PtFeCu}/SA_O{}^{PtFe}$ ratio (1.2) [33], that is, substantially the addition of Cu has the same effect on the SA of ordered and disordered PtFe catalysts. This is an interesting results: indeed, considering that disordered ternary catalysts for the ORR were widely studied [9], the best ternary catalyst compositions observed in disordered form should be also tested in the ordered form.

References

[1] E. Antolini, Recent developments in polymer electrolyte fuel cell electrodes, J. Appl. Electrochem. 34 (2009) 563–576.
[2] C. Wang, S. Wang, J. Zhang, J. Li, M. Ouyang, J. Wang, The key materials and components for proton exchange membrane fuel cell, Progr. Chem. 27 (2015) 310–320.
[3] E. Antolini, J.R.C. Salgado, M.J. Giz, E.R. Gonzalez, Effects of geometric and electronic factors on ORR activity of carbon supported Pt–Co electrocatalysts in PEM fuel cells, Int. J. Hydrogen Energy 30 (2005) 1213–1220.
[4] M. Mavrikakis, B. Hammer, J.K. Nørskov, Effect of strain on the reactivity of metal surfaces, Phys. Rev. Lett. 81 (1998) 2819–2822.
[5] P. Strasser, S. Koh, T. Anniyev, J. Greeley, K.L. More, C. Yu, Z. Liu, S. Kaya, D. Nordlund, H. Ogasawara, M.F. Toney, A. Nilsson, Lattice-strain control of the activity in dealloyed core-shell fuel cell catalysts, Nat. Chem. 2 (2010) 454–460.
[6] A. Nilsson, L.G.M. Pettersson, B. Hammer, T. Bligaard, C.H. Christensen, J.K. Nørskov, The electronic structure effect in heterogeneous catalysis, Catal. Lett. 100 (2005) 111–114.
[7] Y.-C. Wang, N. Zhao, B. Fang, H. Li, X.T. Bi, H. Wang, Carbon-supported Pt-based alloy electrocatalysts for the oxygen reduction reaction in polymer electrolyte membrane fuel cells: particle size, shape, and composition Manipulation and their impact to activity, Chem. Rev. 115 (2015) 3433–3467.

[8] R.N. Singh, R. Awasthi, C.S. Sharma, An overview of recent development of platinum-based cathode materials for direct methanol fuel cells, Int. J. Electrochem. Sci. 9 (2014) 5607–5639.
[9] E. Antolini, Palladium in fuel cell catalysis, Energy Environ. Sci. 2 (2009) 915–931.
[10] T.J. Schmidt, Electrocatalysis in polymer electrolyte fuel cells: from fundamentals to applications, ECS Trans. 45 (2012) 3–14.
[11] V.R. Stamenkovic, B. Fowler, B.S. Mun, G. Wang, P.N. Ross, C.A. Lucas, N.M. Markovic, Improved oxygen reduction activity on Pt3Ni(111) via increased surface site availability, Science 315 (2007) 493–497.
[12] S. Mukerjee, S. Srinivasan, M.P. Soriaga, J. McBreen, Role of structural and electronic properties of Pt and Pt alloys on electrocatalysis of oxygen reduction. An *in situ* XANES and EXAFS investigation, J. Electrochem. Soc. 142 (1995) 1409–1422.
[13] E. Antolini, Platinum-based ternary catalysts for low temperature fuel cells: part II. Electrochemical properties, Appl. Catal. B Environ. 74 (2007) 337–350.
[14] S. Guo, S. Zhang, S. Sun, Tuning nanoparticle catalysis for the oxygen reduction reaction, Angew. Chem. 52 (2013) 8526–8544.
[15] P. Strasser, Dealloyed core-shell fuel cell electrocatalysts, Rev. Chem. Eng. 25 (2009) 255–295.
[16] M. Armbrüster, R. Schlögl, Y. Grin, Intermetallic compounds in heterogeneous catalysis—a quickly developing field, Sci. Technol. Adv. Mater. 15 (2014) 034803.
[17] S. Furukawa, T. Komatsu, Intermetallic compounds: promising inorganic materials for well-structured and electronically modified reaction environments for efficient catalysis, ACS Catal. 7 (2017) 735–765.
[18] L. Chen, C. Bock, P.H.J. Mercier, B.R. MacDougall, Ordered alloy formation for Pt_3Fe/C, PtFe/C and $Pt_{5.75}Fe_{5.75}Cu_y/CO_2$-reduction electro-catalysts, Electrochim. Acta 77 (2012) 212–224.
[19] P. Andreazza, V. Pierron-Bohnes, F. Tournus, C. Andreazza-Vignolle, V. Dupuis, Structure and order in cobalt/platinum-type nanoalloys: from thin films to supported clusters, Surf. Sci. Rep. 70 (2015) 188–258.
[20] C. Frommen, H. Rösner, Observation of long-period superstructures in chemically synthesised CoPt nanoparticles, Mater. Lett. 58 (2004) 123–127.
[21] B.W. Roberts, X-ray measurements of order in CuAu, Acta Metall. 2 (1954) 597–603.
[22] Y. Endo, N. Kikuchi, O. Kitakami, Y. Shimada, Lowering of ordering temperature for fct Fe?Pt in Fe/Pt multilayers, J. Appl. Phys. 89 (2001) 7065–7067.
[23] T. Mallát, J. Petró, S. Szabó, L. Marczis, Investigation of Pd + Co alloys by the linear potential sweep method, J. Electroanal. Chem. 208 (1986) 169–173.
[24] L. Peng, E. Ringe, R.P. Van Duyne, L.D. Marks, Segregation in bimetallic nanoparticles, Phys. Chem. Chem. Phys. 17 (2015) 27940–27951.
[25] M. Polak, L. Rubinovich, The interplay of surface segregation and atomic order in alloys, Surf. Sci. Rep. 38 (2000) 127–194.
[26] A.V. Ruban, Surface composition of ordered alloys: an off-stoichiometric effect, Phys. Rev. B 65 (2002) 174201–174204.
[27] Y. Ma, P.B. Balbuena, Pt surface segregation in bimetallic Pt_3M alloys: a density functional theory study, Surf. Sci. 602 (2008) 107–113.
[28] G. Wang, M.A. Van Hove, P.N. Ross, M.I. Baskes, Quantitative prediction of surface segregation in bimetallic Pt-M alloy nanoparticles (M = Ni, Re, Mo), Progr. Surf. Sci. 79 (2005) 28–45.
[29] B.S. Mun, M. Watanabe, M. Rossi, V. Stamenkovic, N.M. Markovic, P.N. Ross, The study of surface segregationstructure, and valence band density of states of Pt3Ni(100),(110), and (111) crystals, Surf. Rev. Lett. 13 (2006) 697–702.
[30] V. Stamenkovic, T.J. Schmidt, P.N. Ross, N.M. Markovic, Surface composition effect in electrocatalysis: kinetics of oxygen reduction on well-defined Pt_3Ni and Pt_3Co alloy surfaces, J. Phys. Chem. B 106 (2002) 11970–11979.
[31] B. Patrick, H.C. Ham, Y. Shao-Horn, L.F. Allard, G.S. Hwang, P.J. Ferreira, Atomic structure and composition of Pt_3Co nanocatalysts in fuel cells: an aberration-corrected STEM HAADF study, Chem. Mater 25 (2013) 530–535.
[32] J. Cho, W. Roh, D.-K. Kim, J.-B. Yoon, J.-H. Choy, H. Kim, X-Ray absorption spectroscopic and electrochemical analyses of Pt-Cu-Fe ternary alloy electrocatalysts supported on carbon, J. Chem. Soc. Faraday Trans. 94 (1998) 2835–2841.
[33] S. Zhang, X. Zhang, G. Jiang, H. Zhu, S. Guo, D. Su, G. Lu, S. Sun, Tuning nanoparticle structure and surface strain for catalysis optimization, J. Am. Chem. Soc. 136 (2014) 7734–7739.
[34] B. Arumugam, T. Tamaki, T. Yamaguchi, Beneficial role of copper in the enhancement of durability of ordered intermetallic PtFeCu catalyst for electrocatalytic oxygen reduction, ACS Appl. Mater. Interfaces 7 (2015) 16311–16321.
[35] Y. Zhang, Z. Duan, C. Xiao, G. Wang, Density functional theory calculation of platinum surface segregation energy in Pt_3Ni (111) surface doped with a third transition metal, Surf. Sci. 605 (2011) 1577–1582.
[36] T. He, E. Kreidler, L. Xiong, E. Ding, Combinatorial screening and nano-synthesis of platinum binary alloys for oxygen electroreduction, J. Power Sources 165 (2007) 87–91.
[37] J.T. Glass, G.L. Cahen Jr., G.E. Stoner, E.J. Taylor, The effect of metallurgical variables on the electrocatalytic properties of PtCr alloys, J. Electrochem. Soc. 134 (1967) 58–64.
[38] K.T. Kim, Y.G. Kim, J.S. Chung, Effect of surface roughening on the catalytic activity of Pt-Cr electrocatalysts for the oxygen reduction in phosphoric acid fuel cell, J. Electrochem. Soc. 142 (1995) 1531–1538.
[39] Z. Cui, H. Chen, W. Zhou, M. Zhao, F.J. DiSalvo, Structurally ordered Pt_3Cr as oxygen reduction electrocatalyst: ordering control and origin of enhanced stability, Chem. Mater. 27 (2015) 7538–7545.
[40] D. Wang, H.L. Xin, R. Hovden, H. Wang, Y. Yu, D.A. Muller, F.J. DiSalvo, H.D. Abruna, Structurally ordered intermetallic platinum–cobalt core–shell nanoparticles with enhanced activity and stability as oxygen reduction electrocatalysts, Nature Mater. 12 (2013) 81–87.
[41] L. Zou, J. Li, T. Yuan, Y. Zhou, X. Li, H. Yang, Structural transformation of carbon-supported Pt_3Cr nanoparticles from a disordered to an ordered phase as a durable oxygen reduction electrocatalyst, Nanoscale 6 (2014) 10686–10692.
[42] S. Chen, P.J. Ferreira, W. Sheng, N. Yabuuchi, L.F. Allard, Y. Shao-Horn, Enhanced activity for oxygen reduction reaction on Pt_3Co nanoparticles: direct evidence of percolated and sandwich-segregation structures, J. Am. Chem. Soc. 130 (2008) 13818–13819.
[43] E. Meku, C. Du, Y. Sun, L. Du, Y. Wang, G. Yin, Electrocatalytic activity and stability of ordered intermetallic palladium-iron nanoparticles toward oxygen reduction reaction, J. Electrochem. Soc. 163 (2016) F132–F138.
[44] N. Hodnik, C. Jeyabharathi, J.C. Meier, A. Kostka, K.L. Phani, A. Recnik, M. Bele, S. Hocevar, M. Gaberscek, K.J.J. Mayrhofer, Effect of ordering of $PtCu_3$ nanoparticle structure on the activity and stability for the oxygen reduction reaction, Phys. Chem. Chem. Phys. 16 (2014) 13610–13615.
[45] P. Jovanovič, V.S. Šelih, M. Šala, S.B. Hočevar, A. Pavlišič, M. Gatalo, M. Bele, F. Ruiz-Zepeda, M. Čekada, N. Hodnik, M. Gaberščček, Electrochemical in-situ dissolution study of structurally ordered, disordered and gold doped PtCu3 nanoparticles on carbon composites, J. Power Sources 327 (2016) 675–680.
[46] D. Wang, Y. Yu, H.L. Xin, R. Hovden, P. Ercius, J.A. Mundy, H. Chen, J.H. Richard, D.A. Muller, F.J. DiSalvo, H.D. Abrun˜a, Tuning oxygen reduction reaction activity via controllable dealloying: a model study of ordered Cu_3Pt/C intermetallic nanocatalysts, Nano Lett. 12 (2012) 5230–5238.
[47] C.-H. Cui, H.-H. Li, X.-J. Liu, M.-R. Gao, S.-H. Yu, Surface composition and lattice ordering-controlled activity and durability of CuPt electrocatalysts for oxygen reduction reaction, ACS Catal. 2 (2012) 916–924.
[48] Q. Jia, K. Caldwell, K. Strickland, J.M. Ziegelbauer, Z. Liu, Z. Yu, D.E. Ramaker, S. Mukerjee, Improved oxygen reduction activity and durability of dealloyed $PtCo_x$ catalysts for proton exchange membrane fuel cells: strain, ligand, and particle size effects, ACS Catal. 5 (2015) 176–186.
[49] E. Antolini, Structural parameters of supported fuel cell catalysts: the effect of particle sizeinter-particle distance and metal loading on catalytic activity and fuel cell performance, Appl. Catal. B: Environ. 181 (2016) 298–313.
[50] I. Dutta, M.C. Carpenter, M.P. Balogh, J.M. Ziegelbauer, T.E. Moylan, M.H. Atwan, N.P. Irish, Electrochemical and structural study of a chemically dealloyed PtCu oxygen reduction catalyst, J. Phys. Chem. C 114 (2010) 16309–16320.
[51] V.R. Stamenkovic, B.S. Mun, K.J.J. Mayrhofer, P.N. Ross, N.M. Markovic, Effect of surface composition on electronic structurestability, and electrocatalytic properties of Pt-transition metal alloys: Pt-skin versus Pt-skeleton surfaces, J. Am. Chem. Soc. 128 (2006) 8813–8819.
[52] V.R. Stamenkovic, B.S. Mun, M. Arenz, K.J.J. Mayrhofer, C.A. Lucas, G.F. Wang, P.N. Ross, N.M. Markovic, Trends in electrocatalysis on extended and nanoscale Pt-bimetallic alloy surfaces, Nat. Mater. 6 (2007) 241–247.
[53] P. Strasser, S. Koh, T. Anniyev, J. Greeley, K. More, C. Yu, Z. Liu, S. Kaya, D. Nordlund, H. Ogasawara, m.F. Toney, A. Nilsson, Lattice-strain control of the activity in dealloyed core-shell fuel cell catalysts, Nat. Chem. 2 (2010) 454–460.
[54] A. Pavlisic, P. Jovanovic, V.S. Selih, M. Sala, M. Bele, G. Drazic, I. Arcon, S. Hocevar, A. Kokalj, N. HodnikM. Gaberscek,Atomically resolved dealloying of structurally ordered Pt Nanoalloy as an oxygen reduction reaction electrocatalyst, ACS Catal. 6 (2016) 5530–5534.
[55] B.C. Beard, P.N. Ross Jr., The structure and activity of Pt-Co alloys as oxygen reduction electrocatalysts, J. Electrochem. Soc. 137 (1990) 3368–3374.
[56] S. Koh, M.F. Toney, P. Strasser, Activity?stability relationships of ordered and disordered alloy phases of Pt_3Co electrocatalysts for the oxygen reduction reaction (ORR), Electrochim. Acta 52 (2007) 2765–2774.
[57] A. Bonakdarpour, J. Wenzel, D.A. Stevens, S. Sheng, T.L. Monchesky, R. Lobel, R.T. Atanasoski, A.K. Schmoeckel, G.D. Vernstrom, M.K. Debe, J.R. Dahn, Studies of transition metal dissolution from combinatorially sputtered, nanostructured $Pt_{1-x}M_x$ (M = FeNi; $0 < x < 1$) electrocatalysts for PEM fuel cells, J. Electrochem. Soc. 152 (2005) A61–A72.
[58] F. Maillard, L. Dubau, J. Durst, M. Chatenet, J. André, E. Rossinot, Durability of Pt_3Co/C nanoparticles in a proton-exchange membrane fuel cell: direct evidence of bulk Co segregation to the surface, Electrochem. Comm. 12 (2010) 1161–1164.
[59] J. Greeley, J.K. Nørskov, Electrochemical dissolution of surface alloys in acids: thermodynamic trends from first-principles calculations, Electrochim. Acta 52 (2007) 5829–5836.
[60] E. Antolini, Formation, microstructural characteristics and stability of carbon supported platinum catalysts for low temperature fuel cells, J. Mater. Sci. 38 (2003) 2995–3005.
[61] K. Matsutani, K. Hayakawa, T. Tada, Effect of particle size of platinum and platinum-cobalt catalysts on stability against load cycling, Platinum Met. Rev. 54 (2010) 223–232.
[62] Z. Xu, H. Zhang, H. Zhong, Q. Lu, Y. Wang, D. Su, Effect of particle size on the activity and durability of the Pt/C electrocatalyst for proton exchange membrane fuel cells, Appl. Catal. B: Environ. 111–112 (2012) 264–270.

[63] M. Gummalla, S.C. Ball, D.A. Condit, S. Rasouli, K. Yu, P.J. Ferreira, D.J. Myers, Z. Yang, Effect of particle size and operating conditions on Pt_3Co PEMFC cathode catalyst durability, Catalysts 5 (2015) 926–948.
[64] Y. Shao-Horn, W.C. Sheng, S. Chen, P.J. Ferreira, E.F. Holby, D. Morgan, Instability of supported platinum nanoparticles in low-temperature fuel cells, Top. Catal. 46 (2007) 285–305.
[65] R.M. Darling, J.P. Meyers, Kinetic model of platinum dissolution in PEMFCs, J. Electrochem. Soc. 150 (2003) A1523–A1527.
[66] P.J. Ferreira, G.J. la, O.Y. Shao-Horn, D. Morgan, R. Makharia, S. Kocha, H.A. Gasteiger, Instability of Pt/C electrocatalysts in proton exchange membrane fuel cells. A mechanistic investigation, J. Electrochem. Soc. 152 (2005) A2256–A2271.
[67] M. Watanabe, K. Tsurumi, T. Mizukami, t: Nakamura, P. Stonehart, Activity and stability of ordered and disordered Co-Pt alloys for phosphoric acid fuel cells, J. Electrochem. Soc. 141 (1994) 2659–2668.
[68] Q. Li, L. Wu, G. Wu, D. Su, H. Lv, S. Zhang, W. Zhu, A. Casimir, H. Zhu, A. Mendoza-Garcia, S. Sun, New approach to fully ordered fct-FePt nanoparticles for much enhanced electrocatalysis in acid, Nano Lett. 15 (2015) 2468–2473.
[69] J. Zeng, S. Liao, J.Y. Lee, Z. Liang, Oxygen reduction reaction operated on magnetically-modified PtFe/C electrocatalyst, Int. J. Hydrogen Energy 35 (2010) 942–948.
[70] D.Y. Chung, S.W. Jun, G. Yoon, S.G. Kwon, D.Y. Shin, P. Seo, J.M. Yoo, H. Shin, Y.-H. Chung, H. Kim, B.S. Mun, K.-S. Lee, N.-S. Lee, S.J. Yoo, D.-H. Lim, K. Kang, Y.-E. Sung, T. Hyeon, Highly durable and active PtFe nanocatalyst for electrochemical oxygen reduction reaction, J. Am. Chem. Soc 137 (2015) 15478–15485.
[71] L. Zou, J. Fan, Y. Zhou, C. Wang, J. Li, Z. Zou, Hui Yang, Conversion of PtNi alloy from disordered to ordered for enhanced activity and durability in methanol-tolerant oxygen reduction reactions, Nano Res. 8 (2015) 2777–2788.
[72] H. Liu, M. Dou, F. Wang, J. Liu, J. Ji, Z. Li, Ordered intermetallic PtFe@Pt core–shell nanoparticles supported on carbon nanotubes with superior activity and durability as oxygen reduction reaction electrocatalysts, RSC Adv. 5 (2015) 66471–66475.
[73] H. Schuenburg, E. Muller, G. Khelashvili, T. Roser, H. Bonnemann, A. Wokaun, G.G. Scherer, Heat-treated $PtCo_3$ nanoparticles as oxygen reduction catalysts, J. Phys. Chem. C 113 (2009) 4069–4077.
[74] G. Jiang, H. Zhu, X. Zhang, B. Shen, L. Wu, S. Zhang, G. Lu, Z. Wu, S. Sun, Core/shell face-centered tetragonal FePd/Pd nanoparticles as an efficient non-Pt catalyst for the oxygen reduction reaction, ACS Nano 9 (2015) 11014–11022.
[75] K. Jiang, P. Wang, S. Guo, X. Zhang, X. Shen, G. Lu, D. Su, X. Huang, Ordered PdCu-based nanoparticles as bifunctional oxygen-reduction and ethanol-oxidation electrocatalysts, Angew. Chem. Int. Ed. 55 (2016) 1–7.
[76] C. Wang, D.P. Chen, X. Sang, R.R. Unocic, S.E. Skrabalak, Size-dependent disorder?order transformation in the synthesis of monodisperse intermetallic PdCu nanocatalysts, ACS Nano 10 (2016) 6345–6353.
[77] Y. Matsui, T., Doi, H., Daimon, M. Inaba, Effect of crystallographic ordering in PtCo/C alloy catalyst on durability, Abstract MA2016–02 2639, ECS Meeting MA2016–02 October 2 − 7, 2016, Honolulu, Hawaii.
[78] J. Kim, Y. Lee, S. Sun, Structurally ordered FePt nanoparticles and their enhanced catalysis for oxygen reduction reaction, J. Am. Chem. Soc. 132 (2010) 4996–4997.
[79] J. Wu, S. Shan, J. Luo, P. Joseph, V. Petkov, C.-J. Zhong, PdCu nanoalloy electrocatalysts in oxygen reduction reaction: role of composition and phase properties in catalytic synergy, ACS Appl. Mater. Interfaces 7 (2015) 25906–25913.
[80] H.Y. Kim, S. Cho, Y.J. Sa, S.M. Hwang, G.G. Park, T.J. Shin, H.Y. Jeong, S.D. Yim, S.H. Joo, Self-supported mesostructured Pt-based bimetallic nanospheres containing an intermetallic phase as ultrastable oxygen reduction electrocatalysts, Small 12 (2016) 5347–5353.
[81] L. Xiong, A. Manthiram, Effect of atomic ordering on the catalytic activity of carbon supported PtM (M = Fe, Co, Ni, and Cu) alloys for oxygen reduction in PEMFCs, J. Electrochem. Soc. 152 (2005) A697–A703.
[82] M.V. Lebedeva, V. Pierron-Bohnes, C. Goyhenex, V. Papaefthimiou, S. Zafeiratos, R.R. Nazmutdinov, V. Da Costa, M. Acosta, L. Zosiak, R. Kozubski, D. Muller, E.R. Savinova, Effect of the chemical order on the electrocatalytic activity of model PtCo electrodes in the oxygen reduction reaction, Electrochim. Acta 108 (2013) 605–616.
[83] B. Arumugam, B.A. Kakade, T. Tamaki, M. Arao, H. Imai, T. Yamaguchi, Enhanced activity and durability for the electroreduction of oxygen at a chemically ordered intermetallic PtFeCo catalyst, RSC Adv. 4 (2014) 27510–27517.
[84] H. Kuroki, T. Tamaki, M. Matsumoto, M. Arao, K. Kubobuchi, H. Imai, T. Yamaguchi, Platinum–iron–nickel trimetallic catalyst with superlattice structure for enhanced oxygen reduction activity and durability, Ind. Eng. Chem. Res. 55 (2016) 11458–11466.
[85] T. Tamaki, A. Minagawa, B. Arumugam, B.A. Kakade, T. Yamaguchi, Highly active and durable chemically ordered Pt-Fe-Co intermetallics as cathode catalysts of membrane-electrode assemblies in polymer electrolyte fuel cells, J. Power Sources 271 (2014) 346–353.
[86] C.-E. Kim, D.-H. Lim, J.H. Jang, H.J. Kim, S.P. Yoon, J. Han, S.W. Nam, S.-A. Hong, A. Soon, H.C. Ham, Effect of gold subsurface layer on the surface activity and segregation in Pt/Au/Pt_3M (where M ¼ 3d transition metals) alloy catalyst from first-principles, J. Chem. Phys. 142 (2015) 034707.
[87] X. Li, L. An, X. Wang, F. Li, R. Zou, D. Xia, Supported sub-5 nm Pt–Fe intermetallic compounds for electrocatalytic application, J. Mater. Chem 22 (2012) 6047–6052.
[88] Y. Cai, M. Luo, F. Wang, Z. Sun, H. Zhu, Synthesis of structurally ordered platinum-iron catalysts with enhanced oxygen reduction reaction activity, J.Electrochem 22 (2016) 185–191.
[89] D.-K. Kim, J.-H. Choy, K.-S. Han, S.-J. Hwang, W. Roh, H. Kim, Pt LIII-Edge EXAFS studies on Pt-Cu-Fe alloy electrocatalysts supported on carbon, J. Phys. IV 7 (1997) (C2-953-954).
[90] W. Li, Q. Xin, Y. Yan, Nanostructured Pt–Fe/C cathode catalysts for direct methanol fuel cell: the effect of catalyst composition, Int. J. Hydrogen Energy 35 (2010) 2530–2538.
[91] W. Li, W. Zhou, H. Li, Z. Zhou, B. Zhou, G. Sun, Q. Xin, Nano-stuctured Pt–Fe/C as cathode catalyst in direct methanol fuel cell, Electrochim. Acta 49 (2004) 1045–1055.
[92] Z. Yan, M. Wang, J. Liu, R. Liu, J. Zhao, Glycerol-stabilized $NaBH_4$ reduction at room-temperature for the synthesis of a carbon-supported Pt_xFe alloy with superior oxygen reduction activity for a microbial fuel cell, Electrochim. Acta 141 (2014) 331–339.
[93] R. Loukrakpam, J. Luo, T. He, Y. Chen, Z. Xu, P.N. Njoki, B.N. Wanjala, B. Fang, D. Mott, J. Yin, J. Klar, B. Powell, C.-J. Zhong, Nanoengineered PtCo and PtNi catalysts for oxygen reduction reaction: an assessment of the structural and electrocatalytic properties, J. Phys. Chem. C 115 (2011) 1682–1694.
[94] H. Yang, W. Vogel, C. Lamy, N. Alonso-Vante, Structure and electrocatalytic activity of carbon-supported Pt-Ni alloy nanoparticles toward the oxygen reduction reaction, J. Phys. Chem. B 108 (2004) 11024–11034.
[95] H.R. Colón-Mercado, B.N. Popov, Stability of platinum based alloy cathode catalysts in PEM fuel cells, J. Power Sources 155 (2006) 253–263.
[96] Z. Zhang, M. Li, Z. Wu, W. Li, Ultra-thin PtFe-nanowires as durable electrocatalysts for fuel cells, Nanotechnology 22 (2011) 015602.
[97] A.R. Malheiro, J. Perez, H.M. Villullas, Dependence on composition of electronic properties and stability of Pt–Fe/C catalysts for oxygen reduction, J. Power Sources 195 (2010) 7255–7258.
[98] J. Kim, C. Rong, Y. Lee, J.P. Liu, S. Sun, From core/shell structured FePt/Fe3O4/MgO to ferromagnetic FePt nanoparticles, Chem. Mater. 20 (2008) 7242–7245.
[99] E. Casado-Rivera, D.J. Volpe, L. Alden, C. Lind, C. Downie, T. Vazquez-Alvarez, A.C.D. Angelo, F.J. DiSalvo, H.D. Abruna, Electrocatalytic activity of ordered intermetallic phases for fuel cell applications, J. Am. Chem. Soc. 126 (2004) 4043–4049.